Characterization of optical fibers by digital holographic interferometry

Hamdy H. Wahba[a,b] and Thomas Kreis[b]

[a]Department of Physics, Faculty of Science, University of Mansoura, Damietta, Egypt;
[b]BIAS - Bremer Institut für Angewandte Strahltechnik, Klagenfurter Str. 2, D 28359 Bremen, Germany

ABSTRACT

The refractive index distribution over a cross-section of an optical fiber can differ between core and cladding, can vary over the core in graded index fibers, or may even have a more complicated form in polarization preserving fibers. Besides this intended variations the refractive index may vary due to a loading of the fiber like pressure or bending or due to a faulty production. Digital holographic interferometry is a suitable means for measuring the refractive index distribution. In the experiments reported here the fiber is embedded into an index matching fluid, which is mixed so as to match the index of the cladding. Phase-shifted digital holograms are recorded and the interference phase distribution is calculated. From a single demodulated interference phase distribution the refractive index field is determined by an algorithm based on a model which takes into account the known symmetry of the fiber. It can be shown that the obtained accuracy is better than that of classical two-beam interferometry. Results of experiments with step-index, with graded index, and with polarization preserving fibers are demonstrated.

Keywords: Optical fiber characterization, refractive index fields, fiber bending, digital holography, holographic interferometry, phase shifting

1. INTRODUCTION

Optical fibers are dielectric waveguides which have found numerous applications in communication, in illumination, or as sensors, to name just a few. They have a central core with refractive index n_c, in which the light is guided,[1] embedded in the cladding of slightly lower refractive index n_{cl}, see Fig. 1. The most frequently used

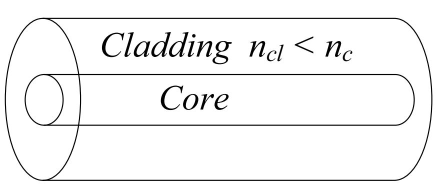

Figure 1. Optical fiber

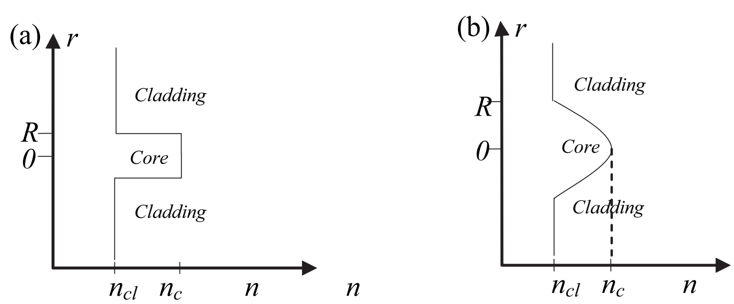

Figure 2. Refractive index distribution in (a) step-index fiber and (b) graded-index fiber

fibers are step index fibers with constant index values in the core as well as in the cladding, se Fig. 2(a). A solution to the problem of modal dispersion[2] is the graded-index fiber with a parabolic or other non-constant distribution of the refractive index in the core, see Fig. 2(b). Due to imperfections and uncontrolled strains in the fiber, a random power transfer between the two polarization directions can occur. Thus linearly polarized light at the fiber input can be transformed into elliptically polarized light. If this effect obstructs the intended

Send correspondence to Th. Kreis, E-mail: kreis@bias.de, Telephone: **49 (0)421 218 5011

Optical Measurement Systems for Industrial Inspection VI, edited by Peter H. Lehmann, Proc. of SPIE
Vol. 7389, 73890K · © 2009 SPIE · CCC code: 0277-786X/09/$18 · doi: 10.1117/12.826854

application, a polarization-maintaining fiber (PM fiber) has to be employed. These fibers typically possess a stress-induced anisotropy in the refractiv index of the core. This anisotropy can be produced by a non-circular cladding cross-section, see Fig. 3(a), or by rods of another material within the cladding as seen in Fig. 3(b). However in all cases the knowledge of the spatial distribution along any cross-section of the fiber is of highest

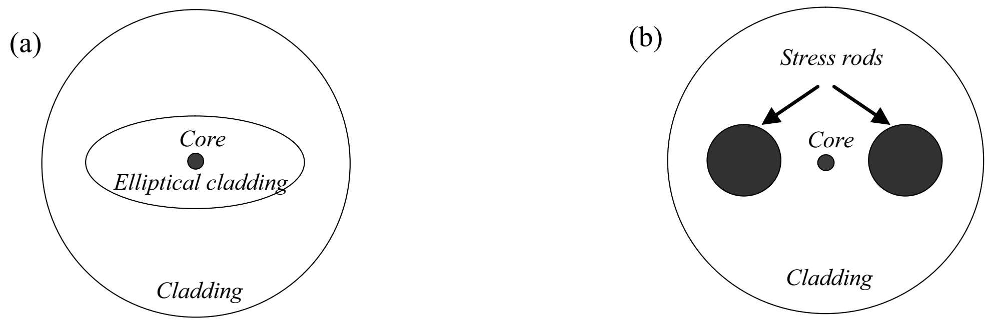

Figure 3. Cross-sections of polarization-maintaining fibers, (a) elliptical clad, (b) Panda type

interest. Since long time, nterferometric methods have been used to measure the refractive index field.[3–8] Their main advantages are their nondestructive nature and the achievable high accuracy.

Here we introduce the fiber characterization by holographic interferometry, where holographically captured and reconstructed wave fields are interferometrically compared. The wave fields are recorded and numerically reconstructed according to the phase shift method in digital holography. The interferometrically measured phase differences correspond to the refractive index variation integrated along the light paths. Since we have strongly varying refractive index fields, refined mathematical models are necessary for an accurate determination of these fields. We therefore here present the slabs-model, which is used for bent optical fibers and the so called multilayer-model, employed for graded index fields. Up to now there is no adequate model for analysing the index fields of the polarization maintaining fibers.

2. HOLOGRAPHIC METROLOGY

Holography is a method for recording and reconstructing three-dimensional complex wave fields, which has found a lot of applications in 3D-imaging, arts advertising, security applications, and in optical testing and metrology.[9] The wavefield O reflected from an opaque surface, scattered by particles, or phase-shifted by a refractive index field is superposed to a coherent reference wave R and the resulting interference intensity I is registered

$$I = (O + R)(O + R)^* = |O|^2 + OR^* + O^*R + |R|^2 \tag{1}$$

For reconstruction the recorded intensity distribution I is illuminated by the reference wave alone and - among others - the original object wave field is restored

$$IR = (|O|^2 + |R|^2)R + O^*R^2 + O|R|^2 \tag{2}$$

Here the last term is the object wave multiplied with a pure intensity term.[10]

2.1 Digital Holography

While in former times the interference between object and reference waves has been recorded on high resolution photographic emulsions, now in digital holography the photographic plates are replaced by CCD or CMOS arrays, and the intensity distributions are digitally stored. Instead of illumination of this so called hologram with the reference wave, the stored hologram now is multiplied with a numerical model of the reference wave.[9] From the product field in the hologram plane, Fig. 4, the field in the image plane is calculated by the diffraction integral

$$b'(x', y') = \frac{1}{\mathrm{i}\lambda} \int\int h(\xi, \eta) r^*(\xi, \eta) \frac{\exp\{\mathrm{i}k\rho\}}{\rho} d\xi \, d\eta \tag{3}$$

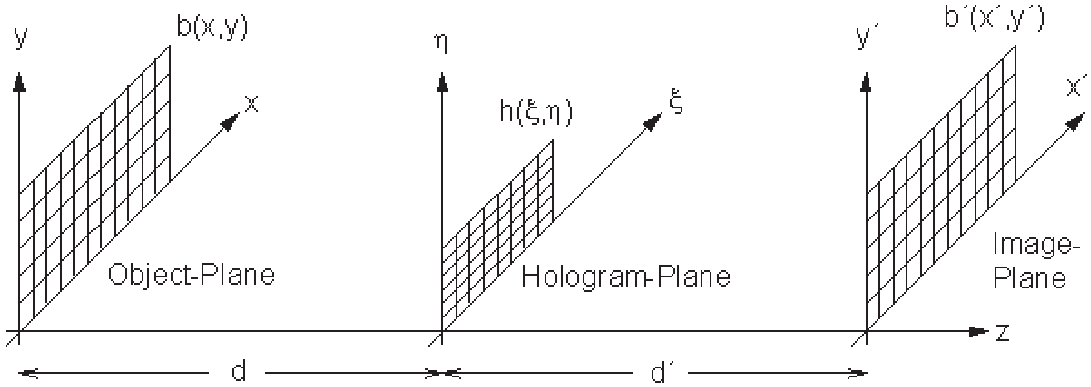

Figure 4. Geometry of digital holography (Explanation of variables in the text)

with λ the used wavelength, $h(\xi, \eta)$ the hologram, $r^*(\xi, \eta)$ the complex conjugate of the reference wave, $\rho = \sqrt{d'^2 + (\xi - x')^2 + (\eta - y')^2}$, and $k = 2\pi/\lambda$ the wavenumber. The coordinates x, y, ξ, η, x', and y' are as shown in Fig. 4. The finite discrete form of the Fresnel approximation to the diffraction integral is[9]

$$b'(n\Delta x', m\Delta y') = A \sum_{j=0}^{N-1} \sum_{l=0}^{M-1} h(j\Delta\xi, l\Delta\eta) r^*(j\Delta\xi, l\Delta\eta) \exp\left\{\frac{\mathrm{i}\pi}{d'\lambda}(j^2\Delta\xi^2 + l^2\Delta\eta^2)\right\} \exp\left\{2\mathrm{i}\pi\left(\frac{jn}{N} + \frac{lm}{M}\right)\right\} \quad (4)$$

This formula calculates the field in the image plane in distance d' from the hologram plane. The $\Delta\xi$ and $\Delta\eta$ are the pixel pitches of the used CCD-array having $N \times M$ pixels. The stored hologram is $h(j\Delta\xi, l\Delta\eta)$. The distance between object and CCD is denoted by d, normally $d' = d$. Complex factors not depending on the hologram under consideration are contained in A. Given a specific CCD the pixel spacing in the reconstructed field is

$$\Delta x' = \frac{d'\lambda}{N\Delta\xi} \qquad \text{and} \qquad \Delta y' = \frac{d'\lambda}{M\Delta\eta} \quad (5)$$

An alternative to the Fresnel approximation uses the fact that Eq. (3) describes a convolution of $h(\xi, \eta) r^*(\xi, \eta)$ with the impulse response $g(x', y', \xi, \eta) = (\exp\{\mathrm{i}k\rho\})/(\mathrm{i}\lambda\rho)$. The convolution theorem now states that b' can be calculated by

$$b' = A'\mathcal{F}^{-1}\{\mathcal{F}\{h \cdot r^*\} \cdot \mathcal{F}\{g\}\} \quad (6)$$

where $\mathcal{F}$ denotes the Fourier transform and $\mathcal{F}^{-1}$ its inverse. In practice both are calculated by the FFT-algorithm. The resulting pixel spacing for this convolution approach is

$$\Delta x' = \Delta\xi \qquad \Delta y' = \Delta\eta \quad (7)$$

2.2 Digital holographic interferometry

From the reconstructed complex fields $b'(x', y')$ the intensity $I'(x', y')$ and phase distributions $\phi'(x', y')$ can be calculated by

$$I'(x', y') = b'(x', y') \cdot b'^*(x', y') \qquad \text{and} \qquad \phi'(x', y') = \arctan\frac{\mathrm{Im}\{b'(x', y')\}}{\mathrm{Re}\{b'(x', y')\}} \quad (8)$$

If we record two digital holograms, one before and one after a phase change in the object wave, e. g. by applying a mechanical stress, varying the load or any physical quantity that changes the refractive index distribution, then the corresponding reconstructed phase distributions can be compared by mere subtraction. Since now in the digital case we know which was the first and which was the second hologram capture, the sign ambiguity of the former double exposure method and optical reconstruction is not any longer present in digital holography. Only the 2π-ambiguity due to the principal value of the arctan-function remains: we obtain a wrapped phase distribution. A practical formula[9] to calculate the phase difference between the two reconstructed fields $b_1'(x', y')$ and $b_2'(x', y')$ is

$$\Delta\phi'(x', y') = \arctan \frac{\mathrm{Im}\{b_2'(x', y' \cdot b_1'^{*}(x', y')\}}{\mathrm{Re}\{b_2'(x', y') \cdot b_1'^{*}(x', y')\}} \tag{9}$$

From this phase difference in practical applications we can then infere on form, deformation, refractive index changes etc.[9]

2.3 Phase shift method in digital holography

If we use a real intensity hologram in the Fresnel or convolution reconstruction we will obtain a strong d.c. term $(|O|^2 + |R|^2)R$, an unsharp virtual conjugate image R^2O^* and a focused real image $|R|^2O$, see Eq. (2). This drawback can be avoided if in the hologram plane of Fig. 4 instead of a real hologram we have the complex wave field O as it is propagated from the object. This complex field can be calculated from several recorded phase shifted holograms in the so called phase shifting digital holography. For this purpose $N \geq 3$ holograms with known mutual phase shifts are recorded. Let these holograms be

$$I_n(x, y) = a(x, y) + b(x, y)\cos[\phi(x, y) + \phi_{Rn}] \qquad n = 1, \ldots, N \tag{10}$$

where $a(x, y)$ and $b(x, y)$ are the additive and the multiplicative distortions and ϕ_{Rn} is the phase shift given to the reference wave during recording of $I_n(x, y)$. An easy phase shift algorithm employs a 90^o phase shift: $\phi_{R1} = 0$, $\phi_{R2} = \pi/2$, $\phi_{R3} = \pi$. The phase distribution then is

$$\phi(x, y) = \arctan \frac{I_1(x, y) - 2I_2(x, y) + I_3(x, y)}{I_1(x, y) - I_3(x, y)} \tag{11}$$

In the experiments described in this paper also a 90^o phase shift is performed, but 4 or 5 holograms are captured with $\phi_{R1} = 0$, $\phi_{R2} = \pi/2$, $\phi_{R3} = \pi$, $\phi_{R4} = 3\pi/2$, $\phi_{R5} = 2\pi$. This approach requires some more effort in capturing two more holograms but pays back by better accuracy and insensitivity with regard to distortions due to redundancy. The phase distribution now is calculated by

$$\phi(x, y) = \arctan \frac{I_4(x, y) - I_2(x, y)}{I_1(x, y) - I_3(x, y)} \tag{12}$$

in the four hologram case and for five holograms by

$$\phi(x, y) = \arctan \frac{7(I_4(x, y) - I_2(x, y))}{4I_1(x, y) - I_2(x, y) - 6I_3(x, y) - I_4(x, y) + 4I_5(x, y)} \tag{13}$$

There are a lot more formulas of this kind.[9] In all cases the numerators and the denominators can be interpreted as the imaginary and the real parts, resp., of the field in the hologram plane. A propagation into the image plane then calculates the complex field without d.c. and virtual terms.

3. NUMERICAL EVALUATION

Digital holographic interferometry like each interferometric method applied to optical fibers gives an interference phase distribution which is due to the integrated refractive index along the optical path.

$$\Delta\phi(x, y) = \frac{2\pi}{\lambda} \int \Delta n(x, y, z)\, dz \tag{14}$$

with $\Delta n(x, y, z) = n_2(x, y, z) - n_1(x, y, z)$ and an optical path parallel to the z-axis. Now inhomogeneous refractive index distributions as well as inclined interfaces between regions of different indices - e. g. between core and cladding or between cladding and environment - lead to a bending of the light rays. This bending is recognized by mathematical models which take into account the geometry of the expected refractive index variation.[11] For bended step index fibers here we introduce the slabs model, for the circular symmetric graded index fibers the multilayer model.

3.1 Slabs model

The slabs model is recommended for the investigation of bent fiber's cladding.[12] Each cross section of the fiber is divided into a number N of equally thick slabs perpendicular to the bending radius. It is assumed that the refractive index is constant in each slab, while it is changing among the slabs, as depicted in Fig. 5. The model

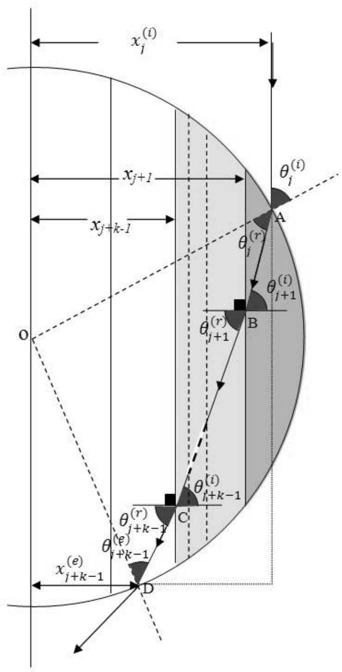

Figure 5. Ray tracing in slabs model

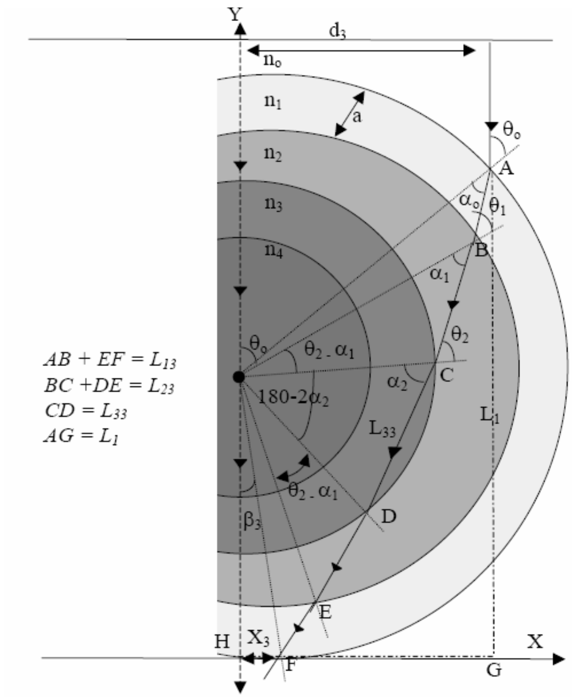

Figure 6. Ray tracing in multilayer model

is based on refraction of light beams at all interfaces to the outside (cladding, liquid, environment) and among the slabs. In the following description the raised indices (i) stand for incident, (r) for refracted, and (e) for emergent beams. Any incident beam enters the slab numbered by j with angle $\theta_j^{(i)}$ with regard to the normal on the interface at distance $x_j^{(i)}$ from the fiber center. Since the refractive index in slab j is n_j, this beam is refracted by angle $\theta_j^{(r)}$. This is the incident angle for the next slab. Finally the beam leaves the fiber at slab $j+k-1$ under angle $\theta_{j+k-1}^{(r)}$ at a distance $x_{j+k-1}^{(e)}$. The approximated optical path length along this beam is

$$\begin{aligned} \frac{\lambda \Delta\phi_k}{2\pi} &= \left[n_j \frac{x_j^{(i)} - x_{j+1}}{\sin(\theta_j^{(i)} - \theta_j^{(r)})} + \sum_{l=j+1}^{j+k-2} n_l \frac{x_l - x_{l+1}}{\cos\theta_l^{(r)}} + n_{j+k-1} \frac{x_{j+k-1} - x_{j+k-1}^{(e)}}{\cos\theta_{l+k-1}^{(r)}} \right] \\ & -n_L \left[\frac{x_j^{(i)} - x_{j+1}}{\tan(\theta_j^{(i)} - \theta_j^{(r)})} + \sum_{l=j+1}^{j+k-2} [(x_l - x_{l+1}) \tan\theta_l^{(r)}] + [(x_{j+k-1} - x_{j+k-1}^{(e)}) \tan\theta_{l+k-1}^{(r)}] \right] \end{aligned} \tag{15}$$

with λ the wavelength of the light beam and $\Delta\phi_k$ the optical phase difference due to refraction in k slabs.

3.2 Multilayer model

The multilayer model is suitable to analyse the core of a graded index optical fiber which is circular symmetric. Therefore we divide a cross-section of the fiber into N circular ring-like layers[4] of equal thickness a. If R is the core radius, we have $N = R/a$. If there is no additional difference in the refractive indices of the clad and the environment, then a recurrence relation predicts the optical path difference of the refracted beam crossing Q of these layers. Let the fiber be illuminated by a collimated beam, with the beam crossing the center of the core defining the optical axis. An arbitrary beam crosses the fiber at distance d_Q from the optical axis and leaves the core at distance x_Q. Then the corresponding fringe shift is given by Z_Q and the optical path difference is

$$\begin{aligned}\frac{\Delta\phi\,\lambda}{2\pi} = \frac{\lambda Z_Q}{h} \quad &= \quad \sum_{j=1}^{Q-1} 2n_j \left(\sqrt{(R-(j-1)a)^2 - d_Q^2 n_L^2/n_j^2} - \sqrt{(R-ja)^2 - d_Q^2 n_L^2/n_j^2}\right) \\ &\quad + 2n_Q \left(\sqrt{(R-(Q-1)a)^2 - d_Q^2 n_L^2/n_Q^2}\right) - \left(\sqrt{R^2 - d_Q^2} + \sqrt{R^2 - x_Q^2}\right) \qquad (16)\end{aligned}$$

with Q between 1 and N and h the interfringe spacing.

4. HOLOGRAPHIC ARRANGEMENT

The holographic arrangement used for the experimental investigations of optical fibers is shown in Fig. 7. Light source is a He-Ne laser with wavelength $\lambda = 632.8\,\text{nm}$ whose beam is filtered and collimatied and crosses a polarizer to get a defined polarization state. The optical fiber is placed on a 2D translation stage and is immersed into an index matching fluid, a mixture of butyl stearate and paraffin oil in a relative concentration that the refractive index of the cladding is exactly met or, if wanted, tuned to a slight mismatch. A microscope objective magnifies the optical field. An identical microscope objective in the reference arm is used to adjust the field curvature. A piezo mounted mirror introduces the phase shifts with respect to the reference wave. The holograms are captured by a CCD camera with pixel pitch $\Delta\xi \times \Delta\eta = 4.65\,\mu\text{m} \times 4.65\,\mu\text{m}$ and pixel numbers 1392×1040.

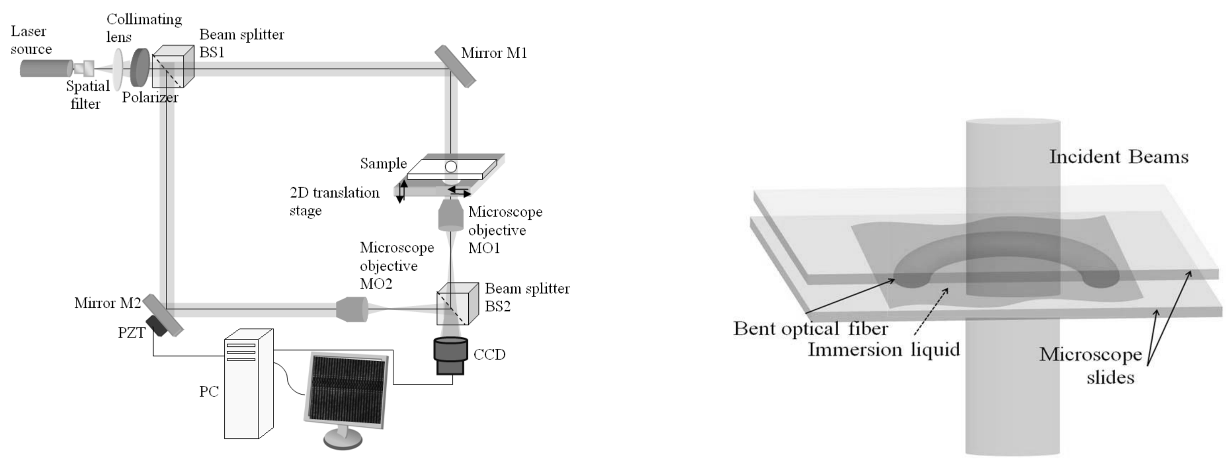

Figure 7. Setup for digital holographic interferometry

5. MEASUREMENT RESULTS

5.1 Bent step-index fibers

First experiments have been performed on bent step-index fibers. Mechanical bending leads to optical birefringence in the optical fiber, so the refractive indices in parallel $n^{\|}$ and perpendicular $n^{\perp}$ directions relative to the optical axis will differ. The mean change in the refractive index occurs in $n^{\|}$ while $n^{\perp}$ is not affected by the mechanical bending.[11,13,14] The fiber here has been stripped, only core and cladding are left. The fiber is immersed into a liquid of $n_L = 1.4598$ which after a variation was found to exactly match the refractive index of the unbent fiber cladding. Two bending radii, $R = 7\,\text{mm}$ and $R = 10\,\text{mm}$ have been used. Phase shifting digital holography with four phase shifted holograms has been employed. The propagation of the light field from hologram plane to image plane has been calculated by the convolution algorithm given in Eq. (6).

Four phase shifted holographic interferograms of a bent optical fiber, bent by a radius $R = 7\,\text{mm}$, with an incident beam parallel polarized with regard to the optical fiber axis are shown in Fig. 8. A tilt of mirror M1 produces carrier fringes oriented perpendicularly to the fiber axis. The reconstructed interference phase modulo 2π is given in Fig. 9(a) where a reconstruction distance -26.99 mm is used.. Digital image enhancement is employed to obtain Fig. 9(b). Then a low order polynomial is fitted to the phase data along the y-direction for each x. We get the background phase map, Fig. 9(c), which is superposed to the original enhanced phase map for a visual check, Fig. 9(d). Unwrapping the phase maps and a subtraction of the background lead to the continuous phase of the bent fiber alone, Fig. 9(e). The results of the same procedure with tilted carrier fringes are

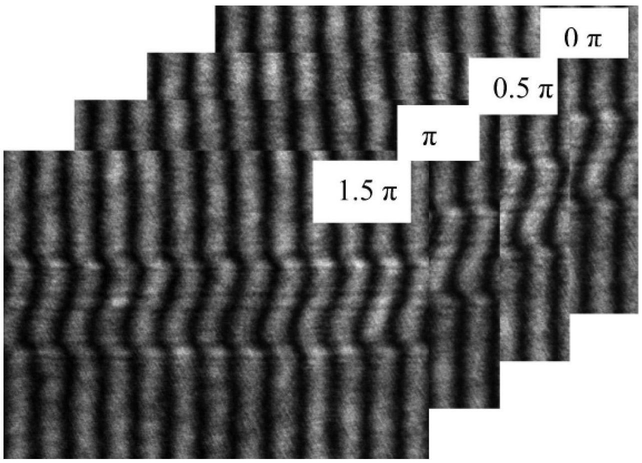

Figure 8. Four phase shifted holographic interferograms of bent optical fiber with bending radius $R = 7\,\mathrm{mm}$. Carrier fringes perpendicular and incident beam parallel polarized to the optical fiber axis

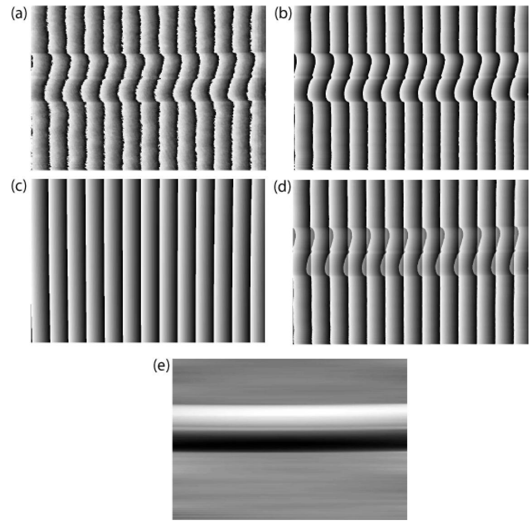

Figure 9. (a) Reconstructed interference phase modulo 2π, (b) enhanced phase map, (c) calculated phase modulo 2π of carrier fringes, (d) superposition of the results of (b) and (c), (e) Interference phase distribution after subtraction

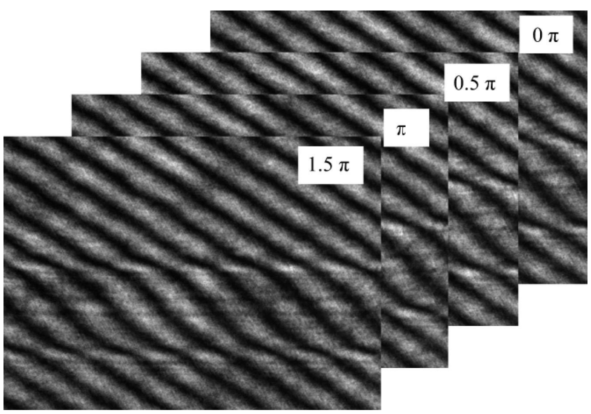

Figure 10. Four phase shifted holographic interferograms of bent optical fiber with bending radius $R = 7\,\mathrm{mm}$. Carrier fringes tilted and incident beam parallel polarized to the optical fiber axis

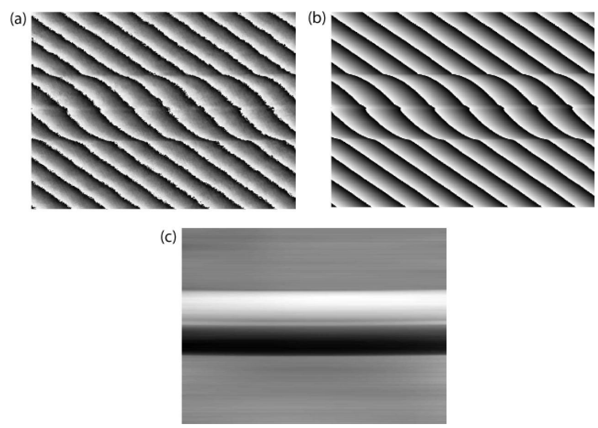

Figure 11. (a) Reconstructed interference phase modulo 2π, (b) enhanced phase map, (c) Interference phase distribution after subtraction

displayed in Figs. 10 and 11. Applying the same evaluation procedure as before we obtain the interference phase distribution of Figs. 11(c) which closely agrees to that of Fig. 9(e). The refractive index profiles of bent optical fibers measured in this way for two different bending radii is seen in Fig. 12.The mean error in the calculated refractive index is 1.11×10^{-4}.The optical birefringence of the bent optical fiber is inversely proportional to the bending radius, but in the border region of the bent fiber cladding there are nonuniform changes in the refractive index as a result of the domination of the liquid in these outmost slabs of the fiber.[13] Therefore reliable results are along a central diameter of $100\,\mu$m in the fiber of diameter $125\,\mu$m.

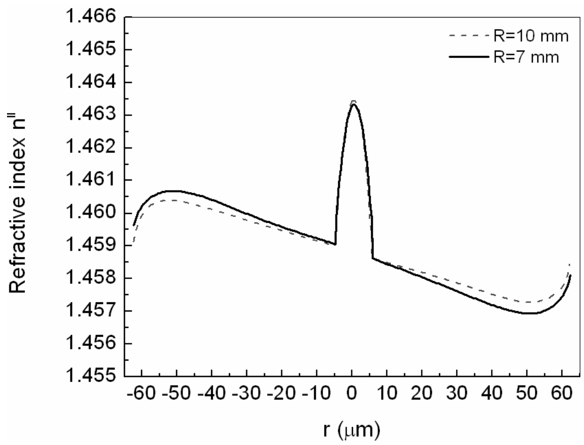

Figure 12. Refractive index profile of bent optical fiber for bending radii R=7mm and R=10mm, fiber radius 62.5 μm

5.2 Graded-index fibers

Another set of experiments was performed on graded-index fibers. Here phase shifting digital holographic interferometry with five phase shifted holograms was used. The first case is with a fluid surrounding the fiber with $n_L = 1.46$ perfectly matching the index of the cladding. The five holograms are shown in Fig. 13 with the reconstructed interference phase distribution modulo 2π in Fig. 14. The distance between hologram plane

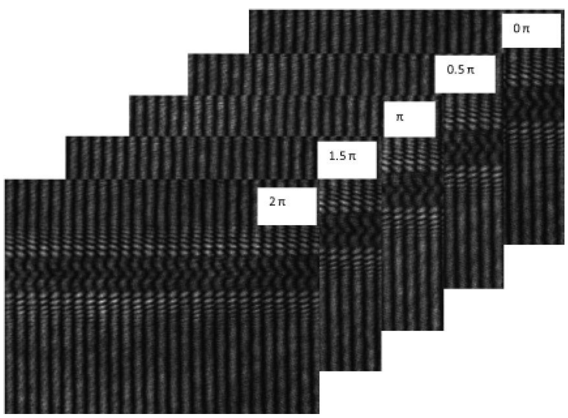

Figure 13. Phase shifted digital holograms of graded index optical fiber immersed in liquid ($n_L = 1.46$) with additional phases (a) 0, (b) $\pi/2$, (c)π, (d)$3\pi/2$, (e)2π

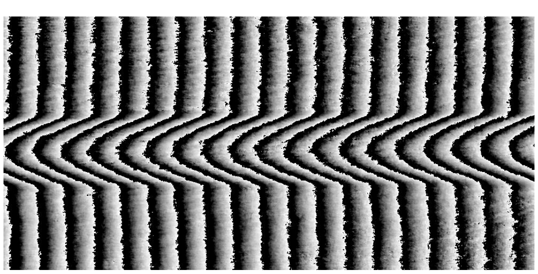

Figure 14. Reconstructed interference phase modulo2π from phase shifted digital holograms of Fig. 13

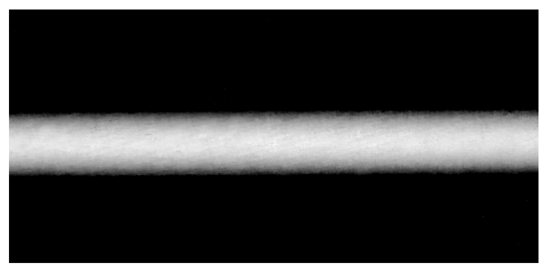

Figure 15. Unwrapped interference phase data of Fig. 13 with normalized background

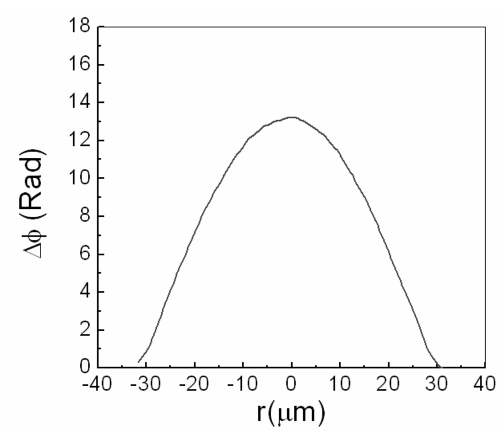

Figure 16. Reconstructed interference phase modulo2π from phase shifted digital holograms of Fig. 13

and image plane here is -150 mm. The phase map after unwrapping and subtraction of the monotonuous background is given in Fig. 15. Finally the mean interference phase difference across the fiber core as calculated by the multilayer model is displayed in Fig. 16. The next example shows the results of the same fiber but for mismatching refractive indices of cladding and liquid. The wrapped phase in Fig. 17, the unwrapped phase with normalized background in Fig. 18, and the phase difference across the fiber in Fig. 19.

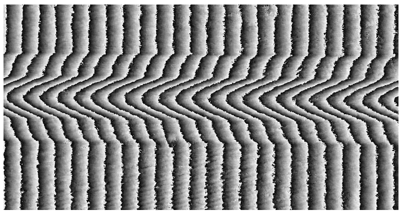

Figure 17. Reconstructed interference phase modulo2π from phase shifted digital holograms

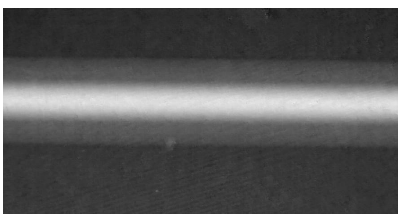

Figure 18. Unwrapped interference phase with normalized background

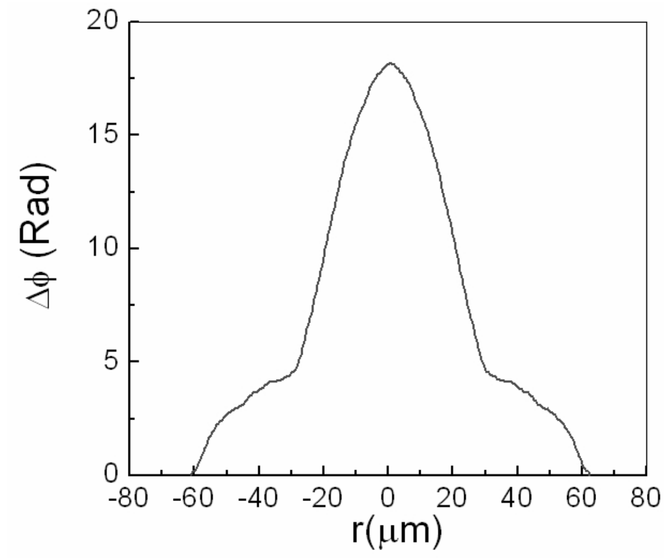

Figure 19. Mean interference phase difference across fiber core relative to liquid for liquid/cladding mismatching

A comparison of the refractive index profiles measured by the digital holographic method introduced in this paper and normal interferometry for matching and mismatching case leads to Figs. 20 and 21. Here the shape parameter α is used to fit the refractive index profile in each case. The mean value of α determined by DHI is 2.0265 ± 0.0696 and it is 1.86 ± 0.07104 when measured by normal interferometry while the exact value is known to be 2.0. This clearly shows that DHI is more accurate than the normal interferometric methods.[11]

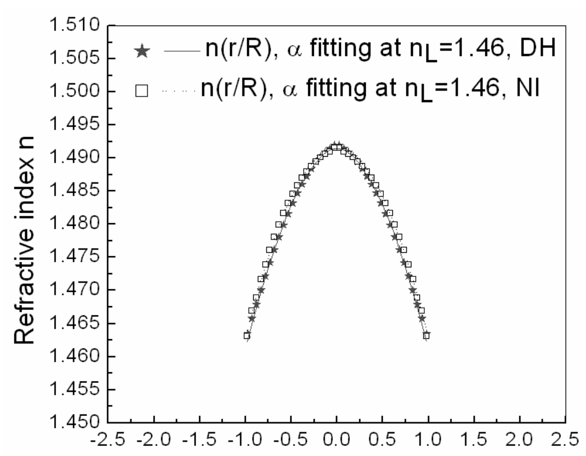

Figure 20. Refractive index profiles across core measured by digital holography (DH) and normal interferometry (NI), matching liquid/cladding

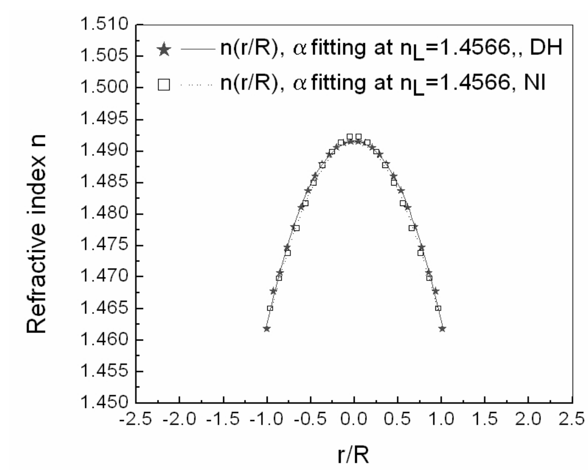

Figure 21. Refractive index profiles across core measured by digital holography (DH) and normal interferometry (NI), mismatching liquid/cladding

5.3 Polarization maintaining fibers

Polarization maintaining optical fibers (PM fibers) are designed to be used in perturbed environments with no or only very small cross coupling of optical power between the propagated polarization modes. DHI also can be used to characterize PM fibers. The polarization state of the incident light beam is selected to be parallel to the optical fiber axis. The fiber sample now is fixed in a rotating device to adjust the fiber axis with respect to the Cartesian coordinates, with the angle zero corresponding to the fast axis of the fiber coincident with the x-axis. Thus the fiber is aligned. Fig. 22 shows four mutually phase shifted holograms of a Panda type PM sample immersed in index matching fluid. The reconstructed phase modulo 2π and the enhanced phase map are given in Figs. 24 (a) and (b) with a distance between hologram plane and image plane of -9.3 mm.. The optical phase difference along the PM fiber is extracted by the subtraction method, Fig. 24 (c). The mean interference phase due to the two stress rods and the core is displayed in Fig. 23. A plot of the optical phase difference along the sample is shown in Fig. 25. A mathematical model for reconstruction of the refractive index distribution from the phase data like the slabs or multilayer model is still lacking. However tomographic methods using interference phase distributions measured from multiple directions exist and will give the desired results.

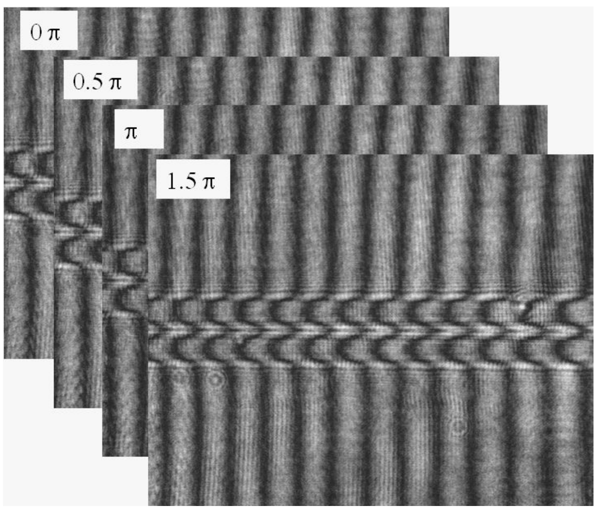

Figure 22. Phase shifted holograms of PM fiber, polarization of incident beam parallel to fiber axis, $N_L = 1.46$

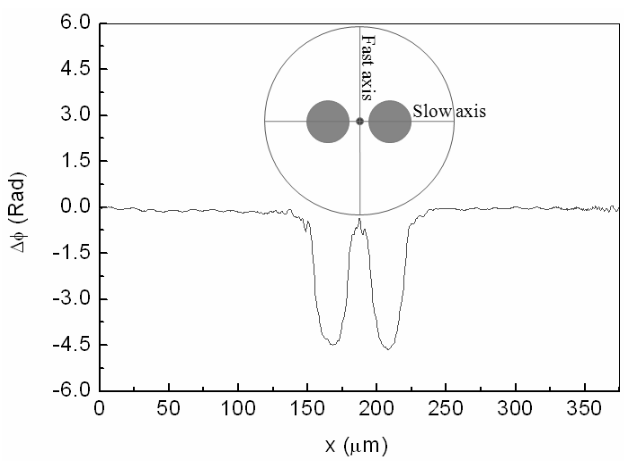

Figure 23. Mean interference phase of the PM fiber

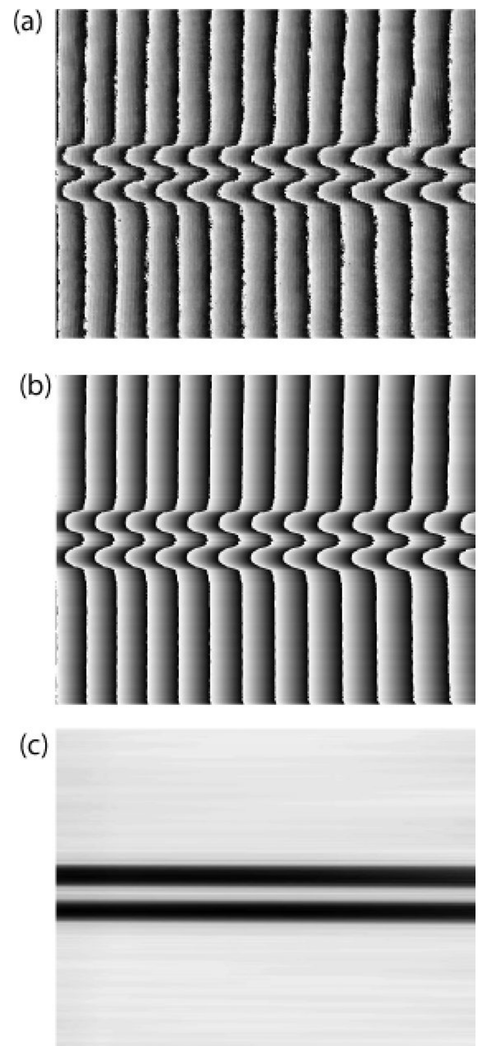

Figure 24. Reconstructed phase (a), enhanced phase map (b), demodulated optical phase difference along the PM fiber (c)

6. CONCLUSIONS

We have shown that digital holographic interferometry is an excellent means to measure optical phase differences induced by refractive index distributions in optical fibers. Due to the high accuracy of the measured phase

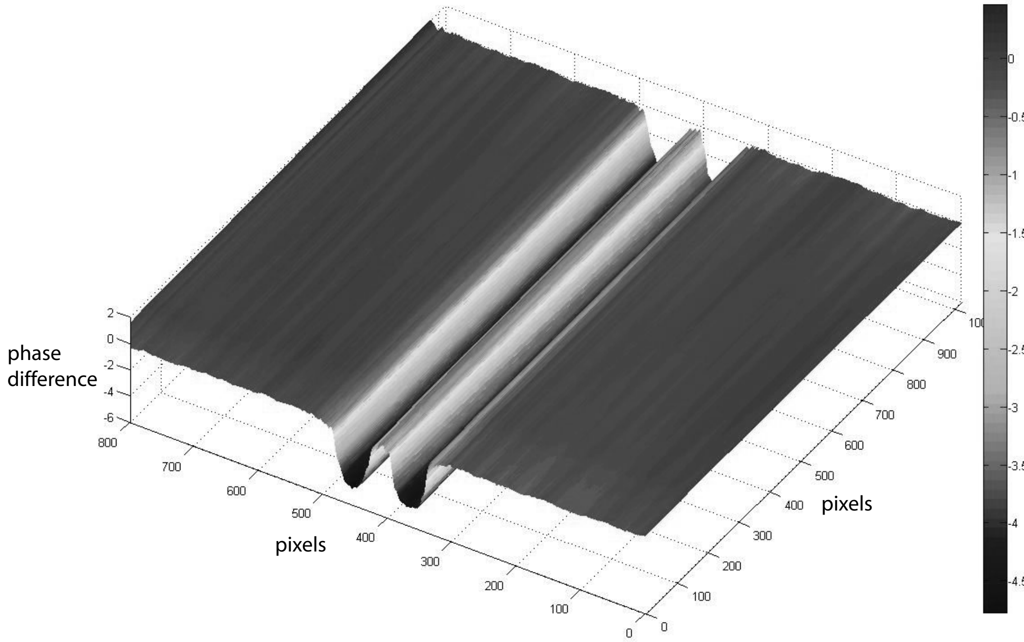

Figure 25. Optical phase difference along PM fiber sample

differences these can be used as input to refined numerical algorithms which calculate the refractive index distribution in the fibers. The method can be applied to a wide variety of fibers, here we have demonstrated the feasibility for bent step index fibers and graded index fibers. The method also can be apllied to polarization preserving fibers but a suitable mathematical model will be developed in future.

7. ACKNOWLEDGEMENTS

H. H. Wahba gratefully acknowledges the sponsoring by the Channel system of the Egyptian government for his stay at BIAS. Furthermore the authors thank A. A. Hamza for fruitful discussions.

REFERENCES

1. G. P. Agrawal, *Fiber-Optic Communication Systems*, J. Wiley and Sons, 2002 (third edition).
2. B. E. A. Saleh and M. C. Teich, *Fundamentals of Photonics*, Wiley Series in Pure and Applied Optics, Hoboken, NJ, 2007 (second edition).
3. A. A. Hamza, T. Z. N. Sokkar, A. M. Ghander, M. A. Mabrouk, and W. A. Ramadan, "On the determination of the refractive index of a fibre. i. skin-core fibre," *Pure Appl. Opt.* **3**, pp. 943–961, 1994.
4. A. A. Hamza, T. Z. N. Sokkar, A. M. Ghander, M. A. Mabrouk, and W. A. Ramadan, "On the determination of the refractive index of a fibre. ii. graded index fibre," *Pure Appl. Opt.* **4**, pp. 161–177, 1995.
5. A. A. Hamza, M. A. Mabrouk, W. A. Ramadan, and M. A. Shams-Eldin, "Determination of grin optical fibre parameters from transverse interferograms considering the refraction of the incident ray by the fibre," *Opt. Commun.* **200**, pp. 131–138, 2001.
6. A. A. Hamza, M. A. Mabrouk, W. A. Ramadan, and H. H. Wahba, "Core-index determination of a thick fibre using lens-fibre interference (lfi) technique," *Opt. and Las. in Eng.* **42**, pp. 121–130, 2004.
7. M. A. El-Morsy, T. Yatagai, A. A. Hamza, M. A. Mabrouk, and T. Z. N. Sokkar, "Multiple-beam fizeau fringe-pattern analysis using Fourier transform method for accurate measurement of fiber refractive index profile of polymer fiber," *J. of Appl. Poly. Sci.* **85**, pp. 475–484, 2002.

8. M. A. El-Morsy, T. Yatagai, A. A. Hamza, M. A. Mabrouk, and T. Z. N. Sokkar, "Automatic refractive index profiling of fibers by phase analysis method using Fourier transform," *Opt. and Las. in Eng.* **38**, pp. 509–525, 2002.
9. T. Kreis, *Handbook of Holographic Interferometry*, Wiley-VCH, Weinheim, 2005.
10. T. Kreis, *Holographic Interferometry: Principles and Methods*, Akademie-Verlag, 1996.
11. H. H. Wahba and T. Kreis, "Characterization of graded index optical fibers by digital holographic interferometry," *Appl. Opt.* **48**, pp. 1573–1582, 2009.
12. T. Z. N. Sokkar, M. A. El-Morsy, and H. H. Wahba, "Automatic fringe analysis of the induced anisotropy of bent optical fibres," *Opt. Comm.* **281**, pp. 1915–1923, 2008.
13. F. El-Diasty, "Interferometric determination of induced birefringence due to bending in single-mode optical fibres," *J. Opt. A: Pure Appl. Opt.* **1**, pp. 197–200, 1999.
14. F. El-Diasty, "Multiple-beam interferometric determination of poisson's ratio and strain distribution profiles along the cross section of bent single-mode optical fibers," *Appl. Opt.* **39**, pp. 3197–3201, 2000.